The high strain rate tension behaviour of pseudo-ductile high performance thin ply composites

Mohamad Fotouhi[1], Jonathan Fuller[2], Marco Longana[2], Meisam Jalalvand[3], Michael R. Wisnom[2]

[1] Department of Design and Mathematics, the University of the West of England, Bristol BS16 1QY, UK

[2] Bristol Composites Institute (ACCIS), University of Bristol, Bristol BS8 1TR, UK

[3] Department of Mechanical and Aerospace Engineering, University of Strathclyde, 75 Montrose Street, Glasgow, G1 1XJ, UK

Abstract

In this study the effect of strain rate in tension on two different types of thin-ply pseudo-ductile laminates is reported. These comprised Unidirectional (UD) and quasi-isotropic (QI) hybrids made from low strain thin-ply carbon/epoxy and high strain glass/epoxy prepreg and all-carbon laminates made from thin-ply [±Θ/0]s laminates referred to as angle-ply (AP) composites. Laminates were designed and subjected to a range of cross-head speeds from 2 mm/min (0.0003 s^{-1}) to 10 m/s (100 s^{-1}). The designed laminates were made from single or hybrids of low strain and high strain unidirectional prepregs, i.e. thin-ply Carbon/epoxy and Glass/epoxy, respectively. Dynamic stress–strain plots and details of the damage mechanisms were obtained for each sample and compared with the quasi-static test results. The investigated thin-ply UD and QI hybrid composite laminates showed excellent pseudo-ductility at different strain rates, whereas the AP laminates were strain rate dependent and pseudo-ductility decreased with increasing strain rate.

Keywords: Pseudo-ductility, Hybrid, Quasi-isotropic, Angle-ply, High strain rate, Thin-ply.

1. Introduction

Nowadays, the use of polymer-matrix composites is increasing very rapidly due to their superior specific structural properties. However, these materials have a sudden brittle failure with a linear elastic response and little warning before failure. This drawback leads to a costly overdesign of composite structures.

Hybridisation of different types of fibres has been found to be a promising method to introduce gradual failure and avoid sudden failure in composite materials [1–5]. Nonlinear pseudo-ductile stress–strain responses, i.e. metal-like behaviour with distinguishable elastic and pseudo-plastic regions, were reported [6-9] for unidirectional (UD) and quasi-isotropic (QI) hybrids made of different types of low strain (glass/epoxy) and high strain (carbon/epoxy) prepregs, when subjected to quasi-static tensile loading condition. This pseudo-ductility was achieved by suppressing the catastrophic delamination and introducing damage mechanisms of (i) low strain material failure/fragmentation, (ii) stable delamination, and (iii) high strain material failure. Material properties, proportion and absolute thickness of the low strain fibre plies are the design parameters to achieve pseudo-ductile UD hybrids. The performance of the pseudo-ductile QI layups was influenced not only by the UD laminates' design parameters but also by the stacking sequence of the plies [9].

Reorientation of the fibres was used as another approach to produce a pseudo-ductile stress-strain behaviour [10-11]. The investigated composites consisting of off-axis and unidirectional thin-ply carbon-fibre reinforced plastic (CFRP) prepregs, arranged as $[\Theta_m/0_n]_s$ layups, showed a metal-like non-linear stress-strain behaviour under quasi-static tensile loading [11]. This behaviour is governed by the gradual failure, via fibre fracture of the central 0-plies and fibre rotation of the off-axis plies. Key parameters of these stress-strain curves, such as laminate modulus, pseudo-ductile strain and strength can all be controlled by adjusting the fibre type, the ratio of angle-ply (AP) to 0 layers and the AP fibre orientation. This gives a certain degree

of flexibility to the performance, giving the potential for a wide range of applications where gradual, stable, rather than sudden, catastrophic failure is paramount.

The response of the pseudo-ductile hybrid and AP laminates under quasi-static loading has been well defined, but in order to design robust and reliable structural components, it is essential to understand the strain rate-dependence of these pseudo-ductile composites. This is particularly important for laminates containing APs, as the relatively highly loaded epoxy matrix is rate dependent and has been shown previously to affect the stress-strain response of the composite [12, 13].

Shokrieh and Omidi [14] did tensile tests on unidirectional glass/epoxy composites at different strain rates, from 0.001 to 100 s^{-1}, and reported increases in tensile strength, modulus, strain to failure and absorbed energy of 52%, 12%, 10% and 53%, respectively. A similar trend was observed for glass/epoxy composites in another study [15]. On the other hand, tensile tests by Taniguchi et al. [16] on unidirectional carbon fibre reinforced plastics under a high strain rate, from 0.001 to 100 $s-1$, demonstrated that the tensile modulus and strength in the longitudinal direction are independent of the strain rate. This is the same tendency as that observed in the study by Harding and Welsh [17]. There are only a few studies on the strain rate effect of glass-carbon/epoxy hybrid composites [18-19]. The combination of these two fibres in conventional hybrids has been found to be strain rate sensitive, due to the rate sensitivity of the glass fibres, with increased stiffness at higher strain rates [20-21].

Angle-ply carbon/epoxy and carbon/S-glass/epoxy laminates/tubes, with $[\pm15]_{2s}$, $[\pm22.5]_{2s}$, $[\pm30]_{2s}$, $[\pm45]_{2s}$, $[\pm60]_{2s}$, $[\pm67.5]_{2s}$ and $[\pm75]_{2s}$ layups, were characterized in pure uniaxial tension (for laminates) and internal pressure (for tubes) at strain rates ranging from quasi-static to over $500s^{-1}$ [22]. In all the case studies, the modulus and strength increase with strain rate, however, ultimate strains did not show any significant trends with strain rate. The effect of

strain rate varies with layup, being lowest for the fibre dominated $[\pm15]_{2s}$ laminates and highest for the matrix dominated $[\pm75]_{2s}$ laminates.

Similar results were presented by Weeks and Sun [13] following high strain rate tensile testing of $[\pm30]_{16s}$ and $[\pm15]_{2s}$ carbon/PEEK specimens. In both cases, the laminates displayed higher strength and modulus with increasing loading rate (1×10^{-5} s^{-1} to 1000 s^{-1}). More recently, tension and compression testing of $[\pm45]_{4s}$ carbon/epoxy (IM7/8552) specimens was carried out by Cui et al [23] to establish the rate-dependence of the in-plane shear response. A large increase in initial modulus and shear stress – prior to the onset of significant non-linearity – was demonstrated when the strain rate was increased from 5 x 10-4 s-1 to 1300 s-1. This behaviour was displayed for both tension and compression. The paper also reports that fibre rotations occur at both strain rates and were incorporated into the calculation of shear stress-strain accordingly.

This paper studies the effect of strain rate in tension, ranging from 2 mm/min (0.0003 s-1) to 10 m/s (100 s-1), in a comprehensive set of tests on pseudo-ductile thin-ply composite laminates. These comprised UD and QI hybrids made from low strain thin carbon/epoxy and high strain glass/epoxy prepreg and also all-carbon laminates made from thin-ply AP $[\pm\Theta/0]s$ laminates. The results showed that the UD and QI hybrid composite laminates have excellent pseudo-ductility at different strain rates. The AP laminates are found to be strain rate dependent, with excellent pseudo-ductility in quasi-static loading and a reduction of pseudo-ductility with increasing strain rate.

2. Experimental procedures

2.1. Materials and specimen design

As listed in table 1, the materials considered in this study were thin carbon prepregs provided by Skyflex and North Thin Ply Technology, and conventional standard thickness glass prepreg

provided by Hexcel. The resin systems could all be cured at 120 ºC, making them compatible in manufacturing and chemical terms. Good integrity of the hybrid laminates was confirmed during test procedures and no phase separation was observed on cross sectional micrographs.

Table 1: Characteristics of the prepregs and fibres applied.

Prepreg type	S-glass/epoxy	USN020A (T300/epoxy)	USN020 (TC35/epoxy)	UIN020 (MR60H/epoxy)	ThinPreg120EPHTg-402 (M55J)
Fibre modulus E (GPa)	88	230	240	290	540
Fibre failure strain (%)	5.5	1.5	1.67	1.9	0.8
Cured nominal thickness (mm)	0.155	0.029	0.022	0.027	0.032
Fibre volume fraction (%)	50	43	50	48	51
Provider	Hexcel	Skyflex	Skyflex	Skyflex	North TPT

Information about the investigated specimen types and lay-up sequences are provided in Table 2. Four types of UD hybrids, one type of QI hybrid and three types of AP laminates were investigated. The UD- G/4C (with a pre-cut)/G configuration has a pre-cut perpendicular to the fibre direction in the T300 carbon layers to study the effect of strain rate on mode II delamination. The AP-$[\pm26_6/0]_s$ layup consisting of Skyflex USN020, AP-$[\pm20_4/0]_s$, and AP-$[\pm22,5_3/0_2/22.5_3]_s$, both comprising Skyflex UIN020 for the $\pm\theta$ plies and North Thin Ply Technology ThinPreg120EPHTg-402 for the 0° plies.

Table 2: Layups of the investigated laminates.

Type	Specimen name	Layup	Thickness (mm)	Number of samples (2 mm/min)	Number of samples (2.5m/s)	Number of samples (5 m/s)	Number of samples (10 m/s)
UD	UD-G/2C/G	$[0_{S\text{-glass}}/0_{C\text{-T300}}/0_{C\text{-T300}}/0_{S\text{-glass}}]$	0.368	5	-	4	4
UD	UD-G/3C/G	$[0_{S\text{-glass}}/0_{C\text{-T300}}/0_{C\text{-T300}}/0_{C\text{-T300}}/0_{S\text{-glass}}]$	0.397	5	-	4	4
UD	UD-G/4C/G	$[0_{S\text{-glass}}/0_{C\text{-T300}}/0_{C\text{-T300}}/0_{C\text{-T300}}/0_{C\text{-T300}}/0_{S\text{-glass}}]$	0.426	5	-	3	4
UD	UD- G/4C(with a pre-cut)/G	$[0_{S\text{-glass}}/0_{C\text{-T300}}/0_{C\text{-T300}}/0_{C\text{-T300}}/0_{C\text{-T300}}/0_{S\text{-glass}}]$	0.426	5	-	4	4
QI	QI	$[60_{S\text{-glass}}/-60_{S\text{-glass}}/0_{S\text{-glass}}/0_{C\text{-T300}}/60_{C\text{-T300}}/-60_{C\text{-T300}}]_s$	1.104	5	-	2	3
AP	AP-$[\pm26_6/0]_s$	$[\pm26_{6C\text{-TC35}}/0_{\,TC35}]_s$	0.572	3	3	3	3
AP	AP-$[\pm20_4/0]_s$	$[\pm20_{4C\text{-MR60}}/0_{C\text{-M55}}]_s$	0.396	3	3	3	3
AP	AP-$[\pm22.5_3/0_2/22.5_3]_s$	$[\pm22.5_{3C\text{-MR60}}/0_{2C\text{-M55}}/\pm22.5_{3C\text{-MR60}}]_s$	0.616	3	3	3	3

The layups were chosen using appropriate values of relative thickness (i.e. proportion of the low strain fibre plies) and absolute thickness of the carbon fibre plies to suppress catastrophic delamination and to obtain three different damage modes of (i) low strain material failure/fragmentation, (ii) delamination, and (iii) high strain material to generate pseudo-ductile response [7-8]. The UD, QI and AP laminates were designed using the damage mode map developed for pseudo-ductile composites [7] to predict their damage mechanisms in quasi-static tension. As an example, the damage mode map with calculated boundaries between the different regions is illustrated in Figure 1, for the investigated UD specimens by considering GIIc=1 N/mm. Regarding the damage mode map of the QI and AP laminates, the multi-directional glass and carbon sub-laminates were assumed to be homogenised before crack development. Cracks are assumed to propagate through the thickness of the whole carbon/ epoxy laminate. The failure strain of the homogenised materials is assumed to be equal to the fibre failure strain of the 0° layers. This is an acceptable assumption as the stiffness reduction in the deterioration process of the homogenised QI laminate is mainly due to 0° carbon layer

fragmentation. Although this assumption may not be completely accurate due to hybrid effects, it is a reasonable basis to design the configurations.
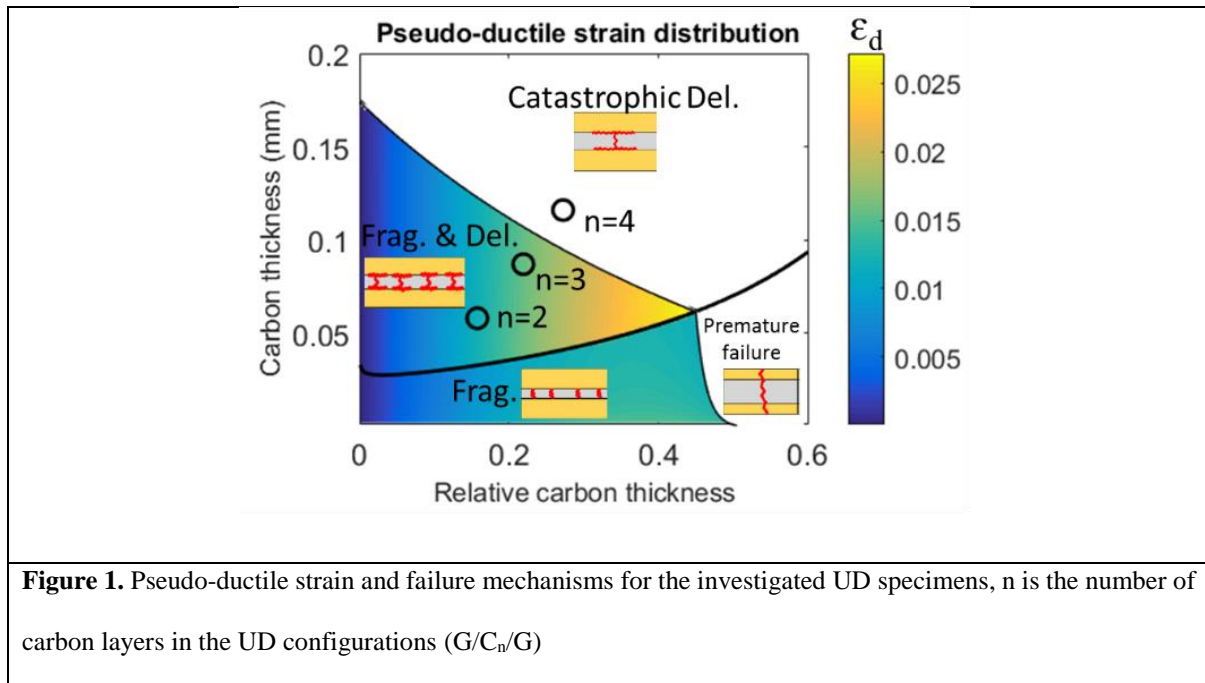

Figure 1. Pseudo-ductile strain and failure mechanisms for the investigated UD specimens, n is the number of carbon layers in the UD configurations (G/C$_n$/G)

2.3. Specimen manufacturing

All the laminates were manufactured via hand layup and autoclave cured as per their resin cure cycles, all having a 120 °C to 125 °C recommended cure temperature by the suppliers. The cured samples were examined using microscope and no phase separation/delamination was observed. Specimens were cut using a diamond-coated cutting wheel. End tabs made of 2 mm thick woven glass/epoxy plates, supplied by Heathcotes Co. Ltd., were bonded to the specimens using a two component Araldite 2000 A/B epoxy adhesive supplied by Huntsman, cured for 120 minutes at 80 °C. The nominal specimen dimensions for the specimens were 240/160/16/h mm overall length/free length/width/variable thickness, respectively.

2.4. Test procedure

Quasi-static testing of the hybrid laminates was performed under uniaxial tensile loading and displacement control using a crosshead speed of 2 mm/min on a computer controlled Instron 8801 type 100 kN rated universal hydraulic test machine with wedge-type hydraulic grips. For better resolution in the expected load range, a 25 kN load cell was attached and used for the measurements. The reason for choosing 2mm/min was to obtain quasi-static behavior of the investigated samples and to compare this behavior with their high strain rate behaviors.

The high-speed tests, run at the strain rates indicated in Table 2, are performed using an Instron VHS 1000, servo-hydraulic test machine, as shown in Figure 2a. The required cross-head displacement speed is achieved by suddenly releasing, through proportional valves, pressurised oil into the actuator. To mitigate the inertial effect, a slack adaptor is placed between the specimen and the actuator allowing the required cross-head displacement speed to be achieved before loading the specimen, as shown in Figure 2b [22].
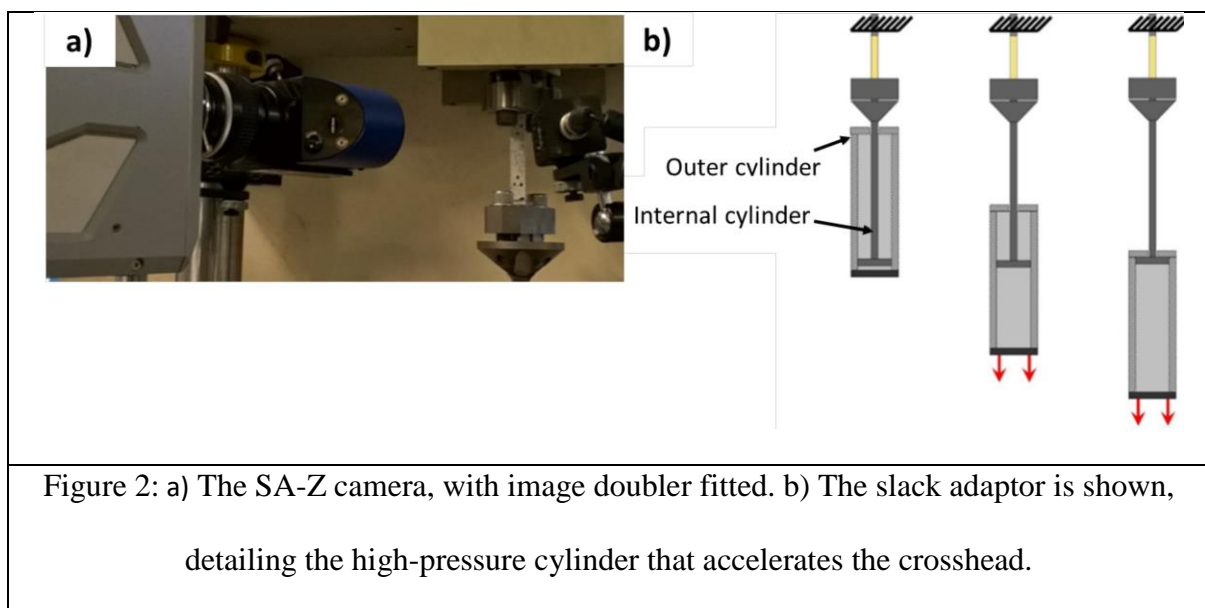
The load was recorded with a 100kN Kistler 9071A washer type piezoelectric load cell attached to the crosshead and coupled with a Kistler Type 5011B charge amplifier. Imetrum video extensometry was used to record strain for the quasi-static tests, whereas all strain field data was recorded using stereo DIC during high strain rate testing. The DIC was performed using a Photron SA-Z camera, fitted with a LaVision Image Doubler that allows stereo images to be captured by a single sensor via mirror and prisms systems. Details about the measurement are provided in Table 3. As a uniform strain field is expected over the specimen surface the strain is calculated as the average of the strain over the whole specimen surface.

It is worth noting that the high rate of the test, coupled with the desire to image the entire specimen that necessitated a frame rate of only 20 kHz (Table 3), limits the number of data points captured by the DIC from initial loading to specimen failure. This can lead to apparent fluctuations in the load-displacement response. Despite these limitations, the data acquired

gives an adequate representation of the response of each specimen, which when considered alongside the image analysis and X-ray CT scanning provides a useful dataset.

Table 3: Digital Image correlation measurement properties

Technique	Digital Image Correlation
Software	DaVis 8.3.1
Subset Size	27 x 27 pixels
Step Size	7 pixels
Camera	Photron SA-Z, 8-bit
Lens	Nikon Nikkor - 50 mm f/1.4D
Filters	LaVision Image Doubler
Resolution	473 x 1032 pixel
Field of View	80.36 x 175.33 mm
Frame Rate	20 kHz
Spatial Resolution	1.19 mm
Strain Resolution	298 $\mu\varepsilon$

Figure 2: a) The SA-Z camera, with image doubler fitted. b) The slack adaptor is shown, detailing the high-pressure cylinder that accelerates the crosshead.

3. Results and discussion

The results are presented in two parts. The first part presents stress-strain behaviour of each configuration at different strain rates. The observed failure modes, microscopy and CT-scans, for the different configurations and strain rates are summarised in the second part.

3.1. Mechanical results

3.1.1. UD and QI samples

Figure 3 shows the in-plane tensile stress–strain results obtained for the UD specimens under quasi-static strain rate. The stress-strain curves show the desired pseudo-ductile behaviour with a linear elastic region, an obvious plateau and a second rising region. In the case of UD-G/2C/G and UD-G/3C/G specimens, the plateau was due to progressive fragmentation of the carbon plies and dispersed delamination of the carbon/glass interface, along the entire gauge length, after the strain reached the strain to failure of the carbon. For the UD-G/4C/G specimens, the plateau was caused by progressive delamination of the carbon/glass interface. After the plateau, once fragmentation and/or delamination were fully saturated, the stress started to increase and the contribution of the carbon plies to the specimen stiffness was diminished and the glass plies carried most of the load. During the second rise, for the UD-G/2C/G and UD-G/3C/G, the glass layers carry most of the increase in load due to saturation of the fragmentation and delamination, and for the UD-G/4C/G the glass carries all the load as the carbon layers have fully delaminated from the glass. By increasing the number of carbon layers, the initial elastic modulus increases, whereas the yield strain/stress and maximum strain/stress show a decreasing trend. With the different number of carbon layers, as a result of the hybrid effect, the carbon plies started to fragment at different strain levels. The thinner ones have a higher strain due to constraint as discussed in [25] by Wisnom et al. The existence of the pre-cut did not have a significant effect on the UD-G/4C/G specimens' mechanical behaviour. This is

because the stress level for the initial carbon ply tensile failure is lower than the stress level for delamination initiation from the pre-cut. The load drops after the start of the plateau and the steady drop in stress, particularly obvious on the lower green trace on Fig. 3, are because of delaminations happening after fragmentation.
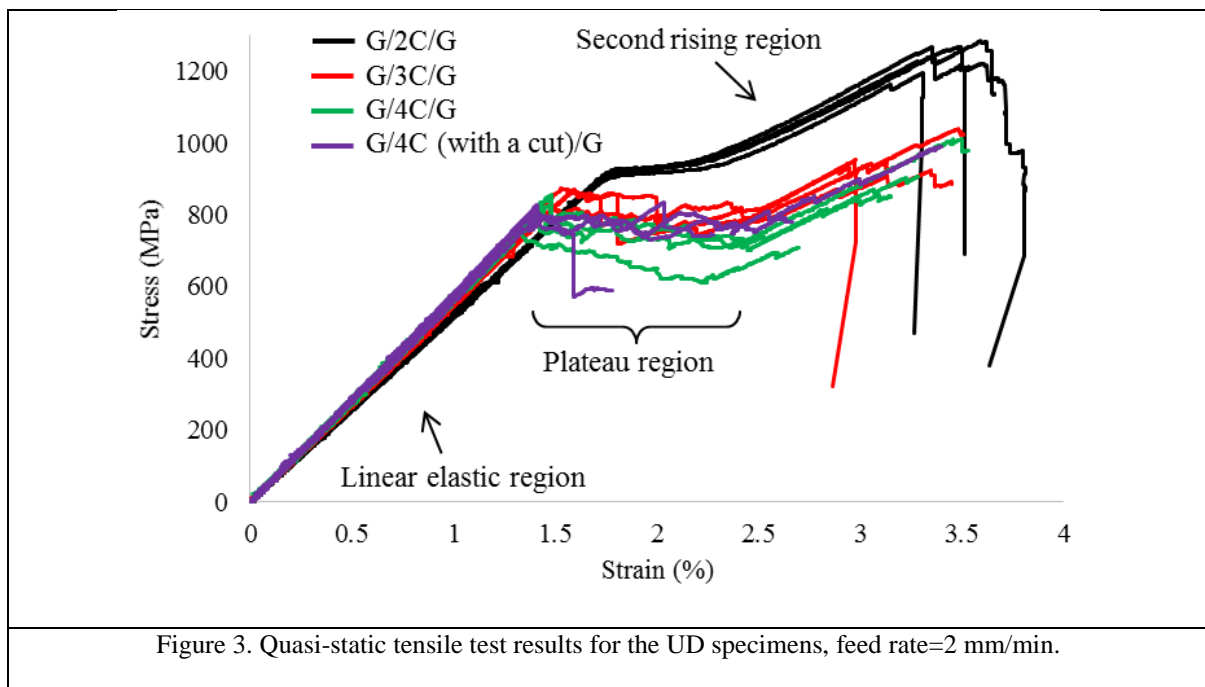
Figures 4 and 5 compare the stress–strain results of the UD and QI samples when subjected to different strain rates. For the quasi-static loading condition, a pseudo-ductile stress-strain curve similar to the UD samples is observable for the QI samples loaded. Some minor damage, i.e. matrix cracking in the off-axis layers, causes a slight non-linearity in the initial slope of the QI samples under the quasi-static loading, as shown in Figure 5.

A slightly longer plateau was observed, when comparing the UD-G/3C/G and UD-G/4C/G with the UD-G/2C/G and QI laminates stress-strain curves. This is because of the higher energy release rates of the UD-G/3C/G and UD-G/4C/G resulting in more delamination compared to the other specimens. Both specimen types show stress–strain curves with small load drops at the beginning of the plateau immediately after the first fracture in the carbon layer.

The overall stress–strain response of the high strain rate tests is relatively similar to the quasi-static results (Figures 4 and 5). The stress–strain trend is approximately linear elastic up to the knee point followed by an obvious plateau and a second rising part. The high scatter can be explained taking into consideration the relatively low sampling frequency that led to obtaining only sparsely populated stress-strain curves. In addition, the dynamic response of the load cell and of the slack-adaptor/specimen assembly, caused the periodic fluctuations in the load signal observable in Figures 4 and 5 [24].

The mean values of the experimental results are summarised in Table 4. For the high strain rate tests, the calculated results are obtained from the laminates that experienced complete cross-sectional failure. The quasi-static tests were stopped when the glass fibres started to split from the edge of the samples.

Generally, as the strain rate increases, there is a strain hardening, so there is an increase in the initial elastic modulus, max-strain and max-stress. It should be noted that the high strain rate data, for all the investigated samples, contains an amount of scatter that makes it difficult to draw any conclusions regarding the percentage of failure strain for the carbon layers (yield strain) and pseudo-ductile strain values.
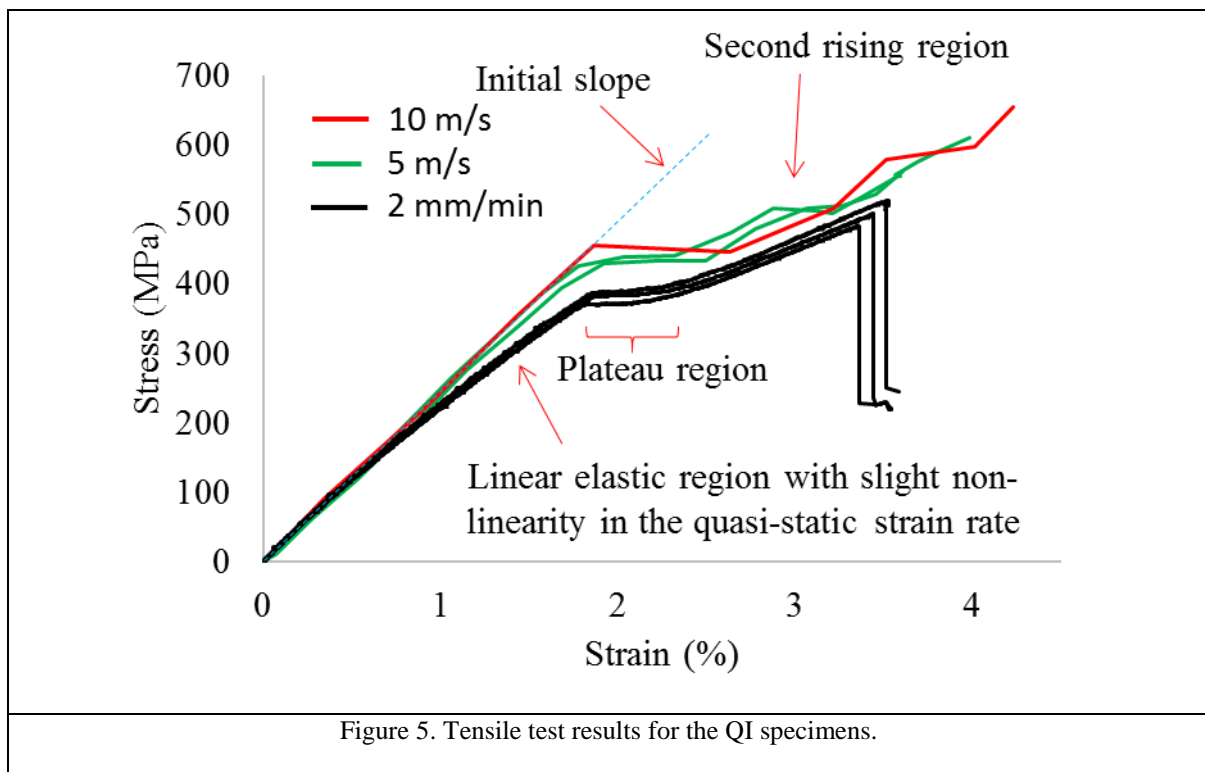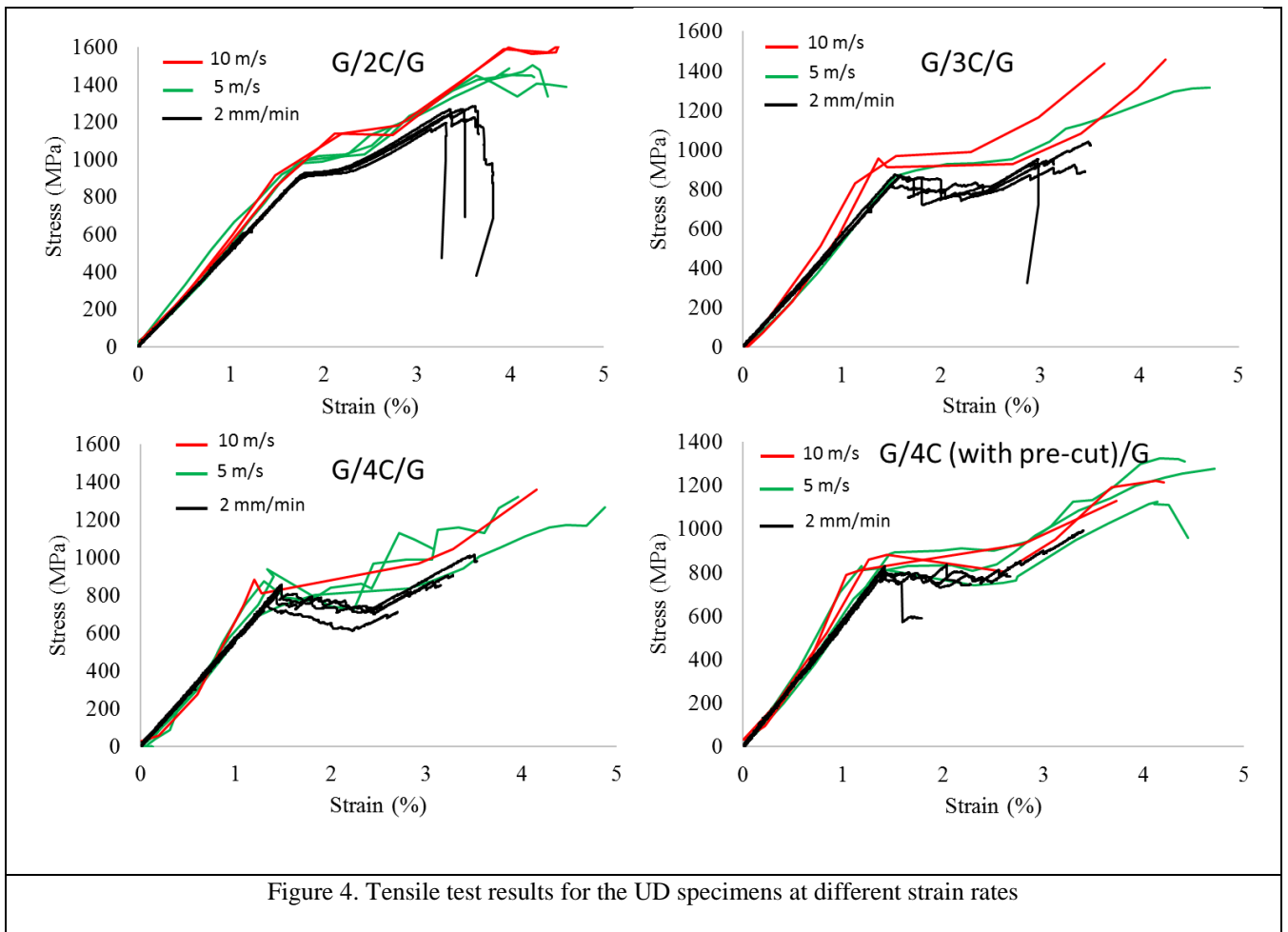

Figure 3. Quasi-static tensile test results for the UD specimens, feed rate=2 mm/min.

Figure 4. Tensile test results for the UD specimens at different strain rates

Figure 5. Tensile test results for the QI specimens.

Table 4. Summary of the results.

* Just one sample was used for the calculations.

Specimen type	Nominal Strain Rate [s^{-1}]	Initial elastic modulus (GPa)	Max-strain (%)	Max-stress (MPa)
UD-G/2C/G	0.00032	52.50±0.1	3.50±0.20	1,260±20
	50	56.30±2.6	4.40±0.18	1,523±30
	100	58.80±2.5	4.82±0.19	1,692±50
UD-G/3C/G	0.00032	56.50±0.5	3.40±0.22	952±40
	50	70.05±15.0	5.07±0.38	1,334±48
	100	76.45±8.5	3.95±0.31	1,444±33
UD-G/4C/G	0.00032	57.60±0.5	3.20±0.25	900±35
	50	64.10±7.5	3.96±0.90	1,223±155
	100	70*	4.15*	1,316*
UD- G/4C(with a pre-cut)/G	0.00032	57.60±0.5	2.66*	846*
	50	64.70±9.5	4.42±0.23	1,286±85
	100	76.70±15.0	3.96±0.24	1,215±110
QI	0.00032	23.50±0.1	3.5±0.10	504±18
	50	23.70±0.1	3.8±0.26	585±32
	100	23.80*	4.23*	655*

3.1.2. AP samples

The test results from each AP configuration are illustrated in Figure 6 at different strain rates. Unlike the UD and QI samples, the AP samples showed strain rate dependent trends.

3.1.2.1. AP-[±26$_6$/0]$_s$

For this layup the quasi-static tests produced a considerable pseudo-ductility, as detailed in Figure 6. Key parameters of the behaviour are given in Table 5. Figure 6 shows clearly that the total amount of pseudo ductility was dramatically reduced at the high strain rates. Initial stress-strain responses are similar but overall the specimens retained stiffness and exhibited

considerably higher strengths, with limited non-linearity. The modulus and strength increased by 20% and 30% respectively from the quasi-static to $100s^{-1}$ strain rate. For strain rates of 50 s^{-1} and 100 s^{-1}, the stress-strain behaviour is predominantly linear, which means it is difficult to say with certainty if fragmentation took place prior to failure. This is unlikely for specimens #8 and #9, as the stress-strain curves are linear to failure.

3.1.2.2. *AP-[±20$_4$/0]$_s$*

As shown in Figure 6, the quasi-static results showed a consistent pseudo-ductility from the AP-[±20$_4$/0]$_s$ specimens. The rate dependence of the specimens resulted in progressively lower pseudo-ductile strain with the increase in strain rate (see Figure 6.). A key result is the effect of the strain rate on the initial modulus. Unlike the AP-[±26$_6$/0]$_s$ configuration, after an increase in the initial modulus from the quasi-static strain rate, there is no meaningful change for all further increases in strain rate. This is likely caused by the use of high modulus fibres for the 0° plies, coupled with the low strain values in the angle-ply layers that will limit non-linearity in those plies. There is a large mismatch in modulus between the M55J and MR60 fibres and, as such, the M55J fibres dominate the initial response of the laminate. This, coupled with the insensitivity of carbon fibres to strain rate effects, means that the rate dependency of the off-axis plies in the AP-[±20$_4$/0]$_s$ specimens are much less than those in the AP-[±26$_6$/0]$_s$ specimens.

3.1.2.3. *AP-[±22.5$_3$/0$_2$/±22.5$_3$]$_s$*

The results for the AP-[±22.5$_3$/0$_2$/±22.5$_3$]$_s$ laminate, Figure 6, are similar to those seen for AP-[±20$_4$/0]$_s$ with similar fibres. In this case, the ±22.5$_3$ fibres lead to a lower level of max-strain for the quasi-static strain rate. The same trend of reducing pseudo-ductility with increasing

strain rate is seen again, though in this case the pseudo-ductility is not cut so drastically. Unexpectedly, the highest strain rate of 100 s^{-1} displays more pseudo-ductility than the 50 s^{-1} rate. Importantly, however, neither of these strain rates causes the same level of non-linearity as the specimens tested at 25 s^{-1}. The stress-strain response, Figure 6, shows a large reduction in modulus at the initiation of fragmentation, which is followed by a section of further loading up to failure at a mean strength of 1005MPa. It should be noted that there is a significant amount of stress fluctuation in the response of the 25 s^{-1} specimens following the onset of non-linearity. As discussed in Section 2.4, this is considered to be an artefact from the testing machine, the dynamic nature of the test and the low number of data points captured by the DIC.

Across all the AP specimens, the strains to failure at high rates were considerably less than observed for the quasi-static tests. The rate dependence of the epoxy resin is thought to contribute to this phenomenon via an increased shear stress in the angle plies. This change in the shear response of the off-axis plies directly affects the behaviour of the laminate as a whole. The shear stress developed in the AP layers is linked to the off-axis angle – a larger fibre angle leading to higher in-plane shear stresses. At quasi-static rates, the shear stress is relatively low until after fragmentations and dispersed delaminations develop and fibre rotations occur. This means that the fibre angle mainly contributes to the final failure of the fully fragmented laminate. The demonstrated rate sensitivity means that the AP layup optimal for quasi-static loading may not the best option for a high strain rate condition.
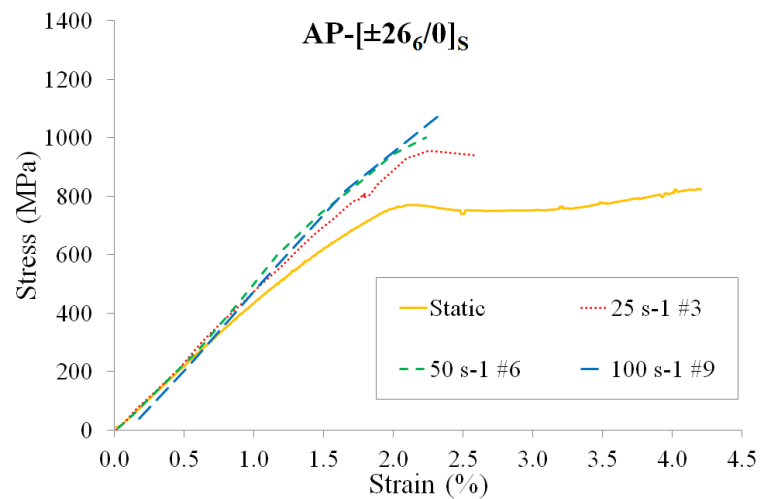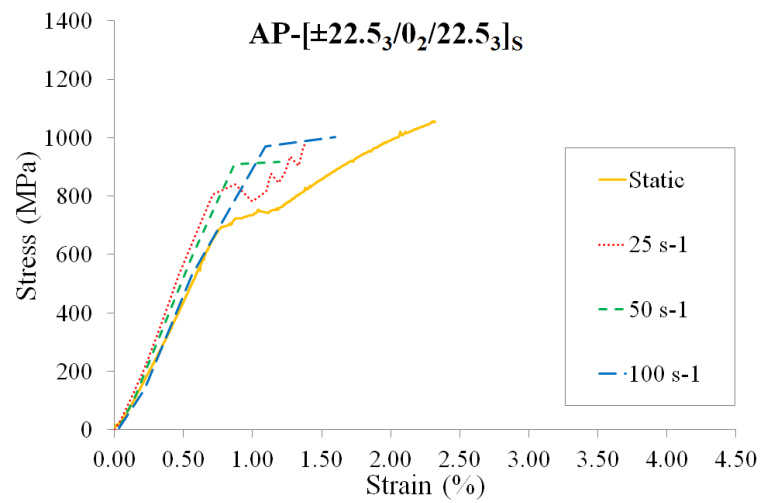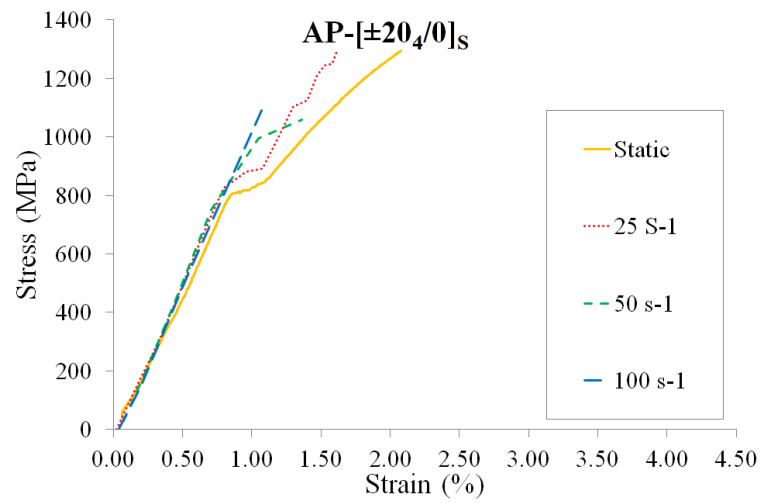
Figure 6: Typical stress-strain results for the tested AP specimens at each nominal strain rate.

Table 5: Experimental values for key parameters of all the AP specimens.

* Just one sample was used for the calculations.

Specimen type	Nominal Strain Rate [s^{-1}]	Initial elastic modulus (GPa)	Max-strain (%)	Max-stress (MPa)
AP-$[\pm26_6/0]_s$	0.00032	45±1	4.24±0.06	838±16
	25	47±2	2.50±0.14	949±24
	50	51±1	2.35±0.17	1019±24
	100	54±2	2.49±0.25	1098±27
AP-$[\pm20_4/0]_s$	0.00032	105±1	2.03±0.06	1262±33
	25	112*	1.62*	1291*
	50	112±2	1.31±0.05	1036±24
	100	114±1	1.09±0.03	1104±18
AP-$[\pm22.5_3/0_2/22.5_3]_s$	0.00032	100±2	2.29±0.19	1040±43
	25	112*	1.44*	1005±26
	50	110±1	1.24±0.06	911±8
	100	115±2	1.50±0.15	1034±26

3.2. Damage mechanisms

To aid understanding of the damage evolution and eventual failure process of the investigated laminates, high and low speed imaging (camera pictures), microscopy and X-ray computed tomography were performed. The results are summarised below.

3.2.1. UD and QI samples

The observed failure mechanisms in high-strain tests, captured using high speed videos, show a similar pattern to quasi-static. These damage mechanisms, i.e. dispersed fragmentation and dispersed delamination, are observable on the specimens' surfaces from Figures 7 to 11. The delaminated back surface of the glass layer blocked the visibility of the carbon, therefore, the

fragmentation cracks and the delaminated nearby region were visible through the translucent glass ply.

The damage evolution of the UD-G/2C/G, UD-G/3C/G and QI laminates is similar to each other: initially the carbon fibres started to fragment just before the first smooth knee in the stress-strain graphs (Figures 4 and 5). This is followed by a plateau region caused by the stable progressive carbon plies fragmentation and localised delamination of the fragmented carbon plies.

For the UD specimens with four plies (with cut and without cut) subjected to quasi-static strain rates, Figures 9a and 10, due to the higher energy release rate, the first carbon fragmentation is followed by a load-drop and progressive delamination growth, i.e. the pull-out of the carbon layers without further fragmentation, this translates into a slightly decreasing plateau on the stress-strain curves of Figure 3. The UD-G/4C/G specimens with the pre-cut (see Figure 10) did not show a difference in damage mechanisms as they did not delaminate from the cut. From this figure, it seems that a carbon layer failure occurred underneath the black painted area close to the grips. This could potentially be due to a small material imperfection at that cross section. The grip pressure was identical for all the quasi-static samples and there were no end tab failures or glass failures in the end tabs.

By increasing the strain rate, the damage mechanisms for the UD-G/4C/G laminates were slightly different (see Figure 9). A progressive delamination growth with limited fragmentation was observed for the quasi-static tests, whereas more carbon ply fragmentations were observed for the high strain rates. This is consistent with the damage mode map prediction (Figure 12.), where by increasing the strain rate, mode II interlaminar fracture toughness increases, so the damage mode changes from overall delamination to stable fragmentation/localised delamination. Figure 11 shows some pictures taken from the broken QI samples after the quasi-

static and high-strain rate tests. A similar damage pattern, i.e. dispersed fragmentation and dispersed delamination, was observed for these applied strain rates.
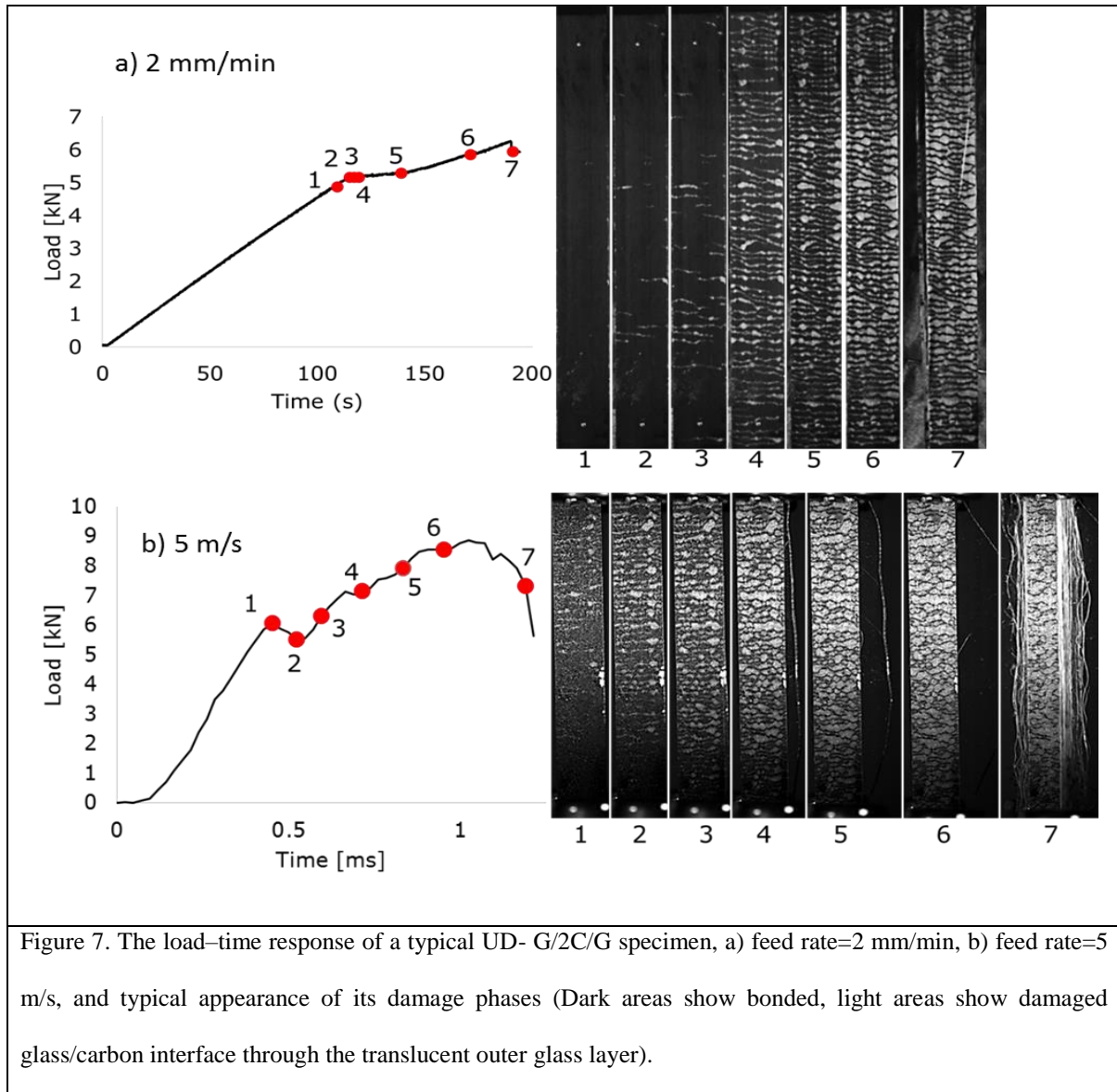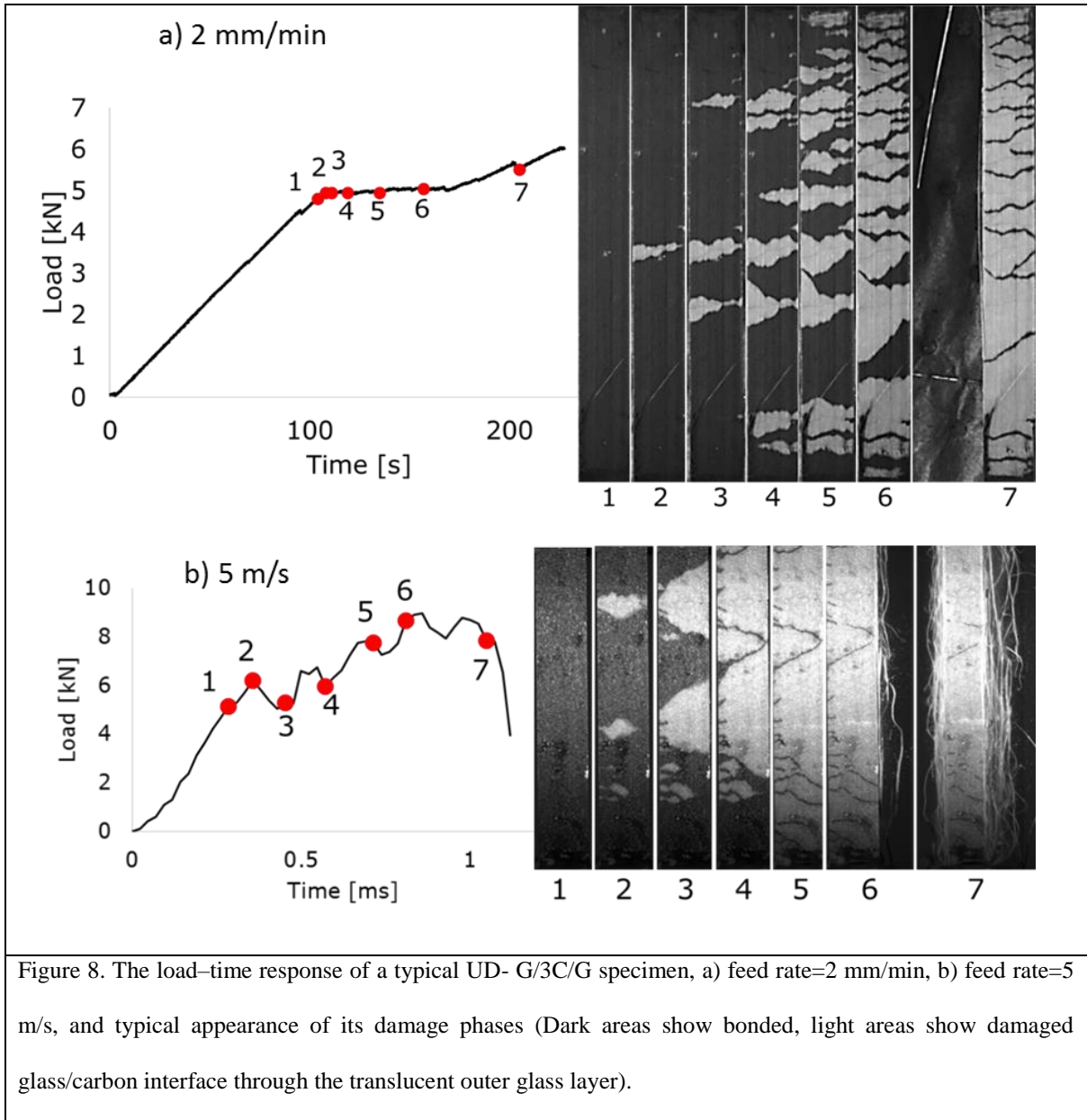

Figure 7. The load–time response of a typical UD- G/2C/G specimen, a) feed rate=2 mm/min, b) feed rate=5 m/s, and typical appearance of its damage phases (Dark areas show bonded, light areas show damaged glass/carbon interface through the translucent outer glass layer).
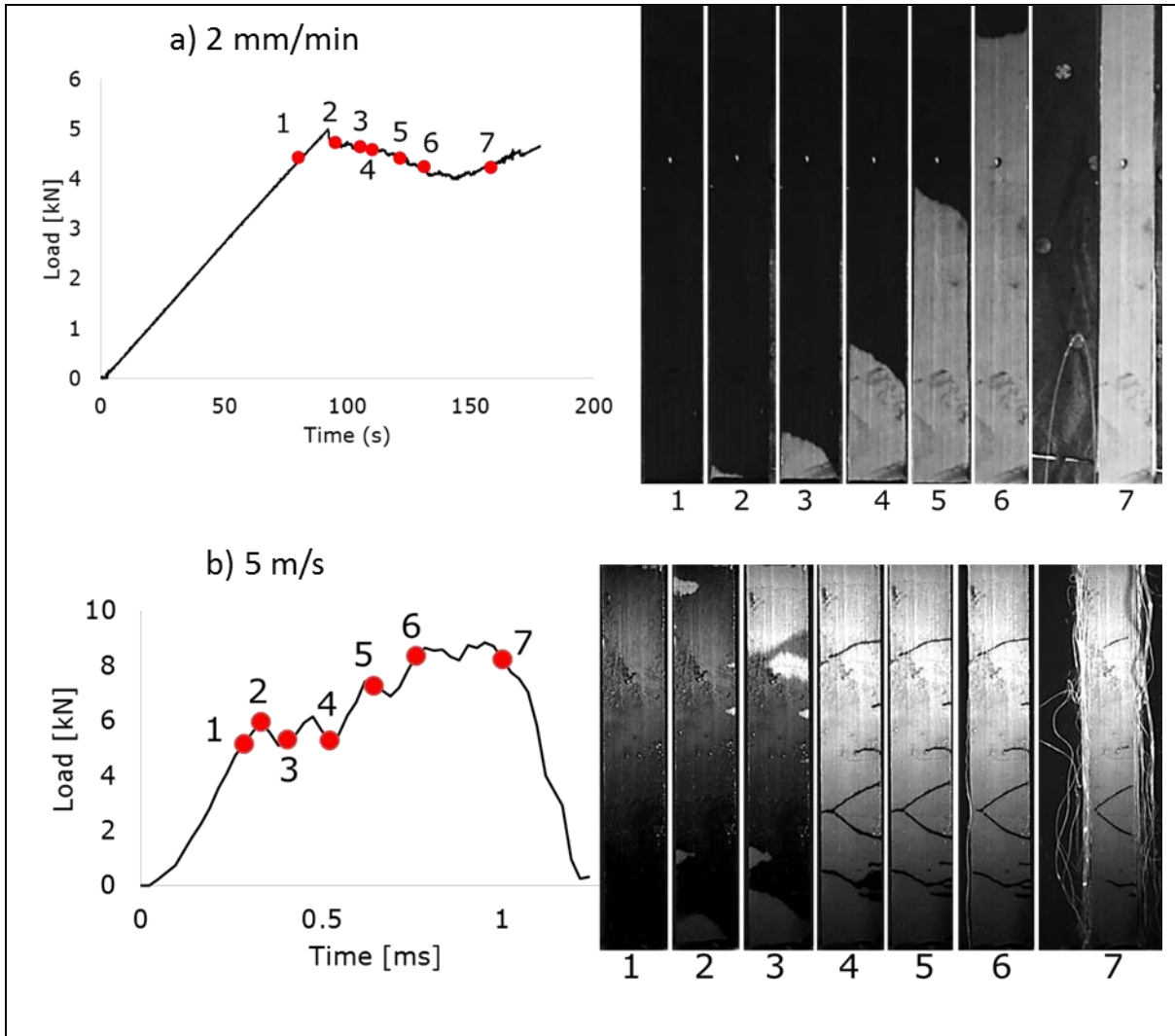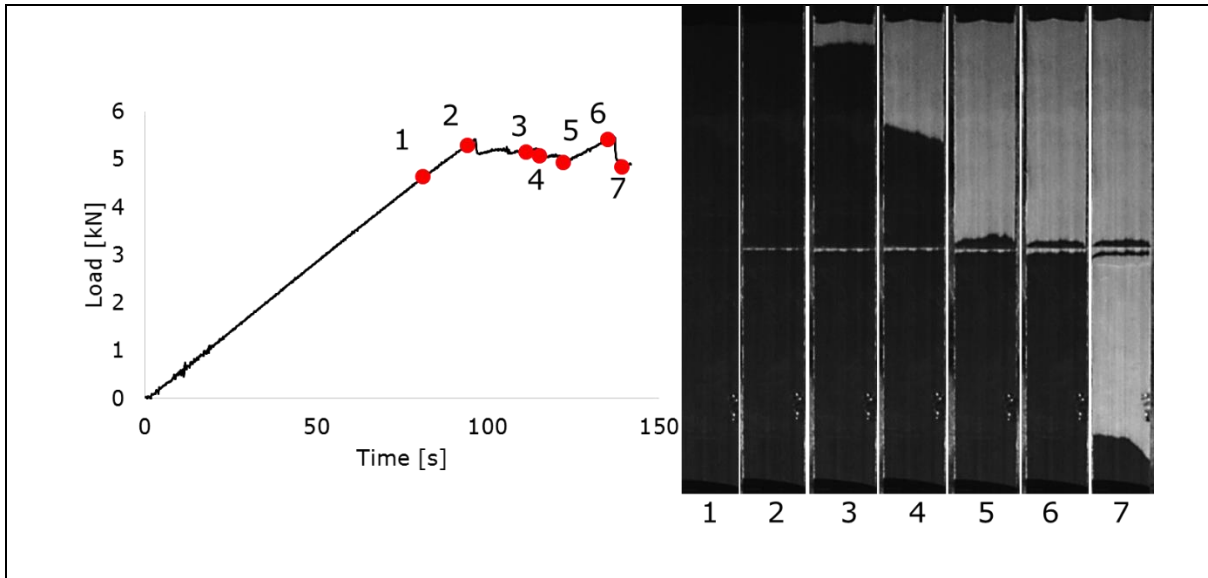
Figure 8. The load–time response of a typical UD- G/3C/G specimen, a) feed rate=2 mm/min, b) feed rate=5 m/s, and typical appearance of its damage phases (Dark areas show bonded, light areas show damaged glass/carbon interface through the translucent outer glass layer).
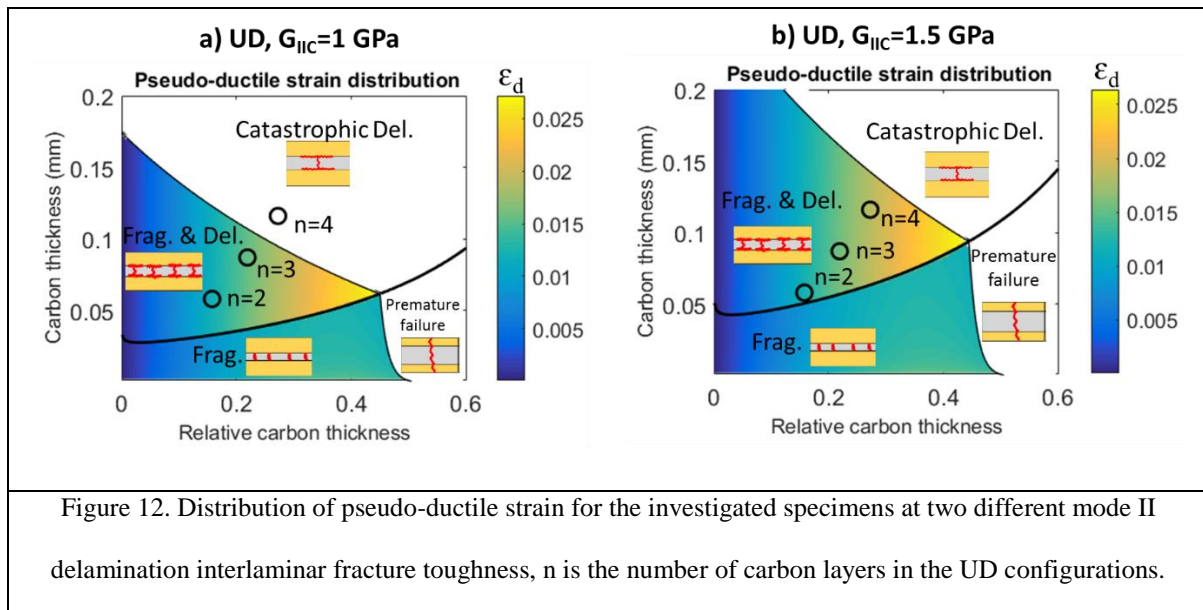
Figure 9. The load–time response of a typical UD- G/4C/G specimen, a) feed rate=2 mm/min, b) feed rate=5 m/s, and typical appearance of its damage phases (Dark areas show bonded, light areas show damaged glass/carbon interface through the translucent outer glass layer).

Figure 10. The load–time response of a typical UD- G/4C (with a pre-cut)/G specimen, feed rate=2 mm/min, and typical appearance of its damage phases (Dark areas show bonded, light areas show damaged glass/carbon interface through the translucent outer glass layer).
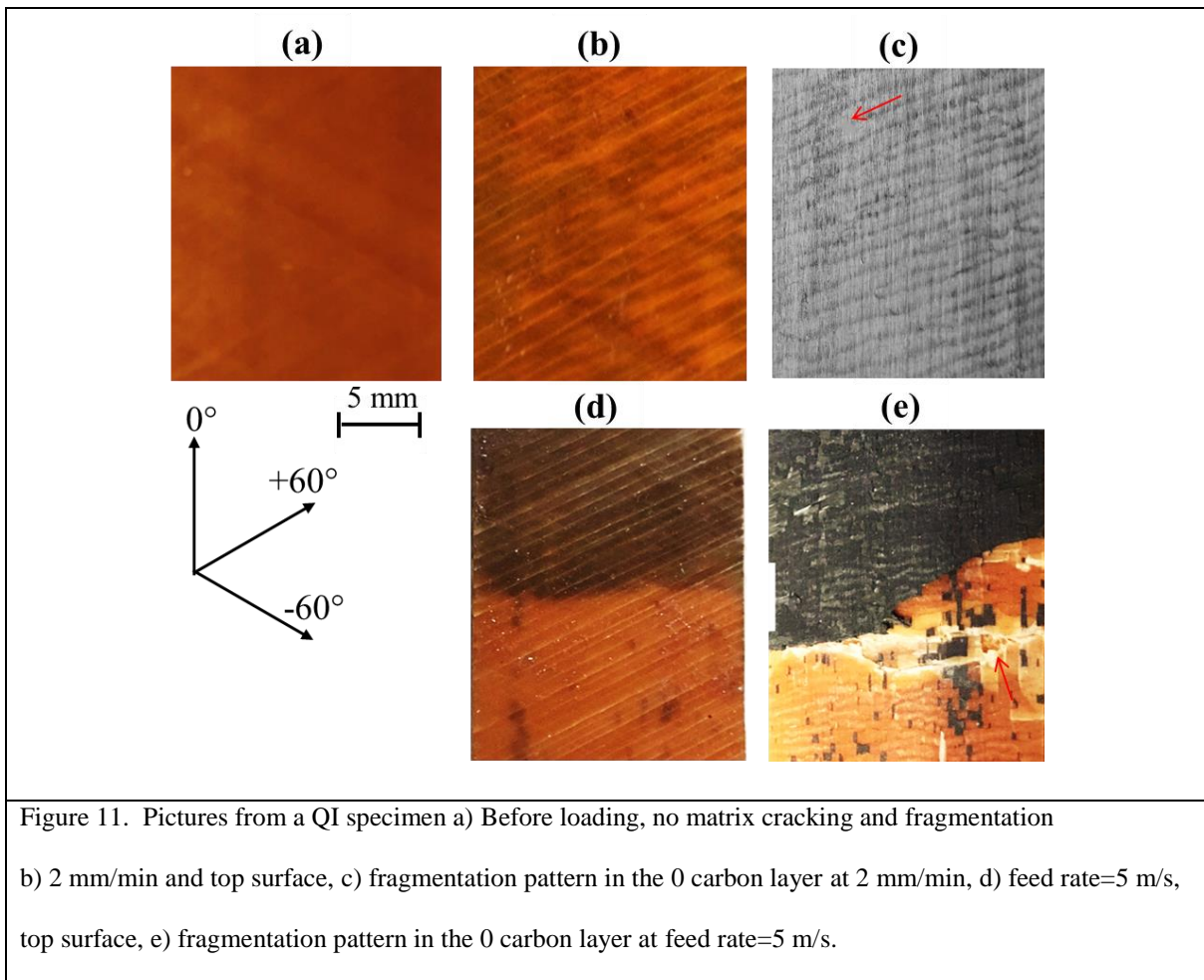
Figure 11. Pictures from a QI specimen a) Before loading, no matrix cracking and fragmentation b) 2 mm/min and top surface, c) fragmentation pattern in the 0 carbon layer at 2 mm/min, d) feed rate=5 m/s, top surface, e) fragmentation pattern in the 0 carbon layer at feed rate=5 m/s.

Figure 12. Distribution of pseudo-ductile strain for the investigated specimens at two different mode II delamination interlaminar fracture toughness, n is the number of carbon layers in the UD configurations.

3.2.2. AP samples

3.2.2.1. Microscopy

Samples were taken for microscopy from tested AP-[$\pm20_4/0$]$_s$ and AP-[$\pm22.5_3/0_2/\pm22.5_3$]$_s$ specimens only. No suitable pieces could be salvaged following the failure of the AP-[$\pm26_6/0$]$_s$ specimens at any of the loading rates.

Figures 13 and 14 show side views (0° fibres running left-right) of representative sections of the *AP*-[$\pm20_4/0$]$_s$ and AP-[$\pm22.5_3/0_2/\pm22.5_3$]$_s$ layups respectively. In each figure the observed locations of fragmentations are highlighted and in Figure 13 these are magnified for a clearer view. Both cases suggest that fragmentations occur sporadically with no regularity to their spacing. The amount of damage surrounding the fibre fractures is minimal, indicating that no delamination occurred at the 0/-θ interfaces following the initiation of fragmentations.

Overall, observing fragmentations and registering their spacing was not straightforward under the microscope. Additionally, it was difficult in some locations to verify if a feature was indeed a fibre fracture caused by testing, or one induced during sample preparation. The microscopy does show that fragmentations occurred, though the images provide little further insight.
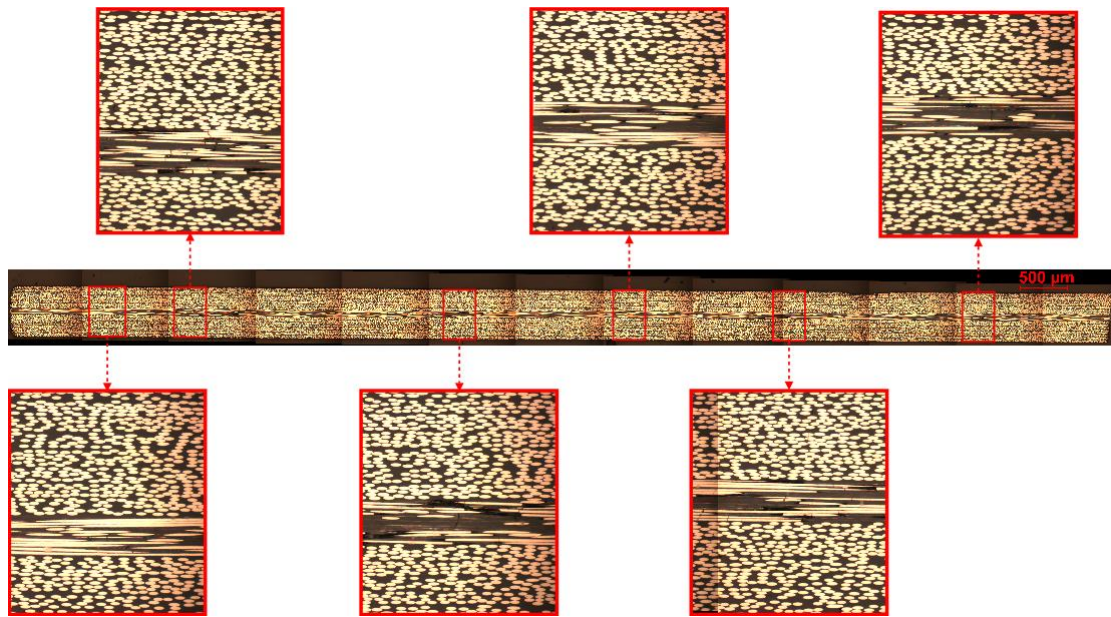
Figure 13: Microscopy for a AP-$[\pm 20_4/0]_s$ specimen tested at 50 s^{-1}. The full width image is a mosaic at 10x magnification. Inset images highlight the locations of fragmentations (20x magnification).

Figure 14: Microscopy for a AP-$[\pm 22.5_3/0_2/\pm 22.5_3]_s$ specimen. The full width image is a mosaic at 10x magnification. Red rectangles highlight the locations of fragmentations.

3.2.2.2. X-ray CT scanning

A number of specimens did not completely fail during testing and these have been imaged using X-ray computed tomography (CT). This was due to the slippage of the specimen in the grips. In total, four specimens were `saved' for CT scanning via this problem: #1 ($\varepsilon_x = 2.4\%$), and #10 (no strain data) AP-$[\pm 26_6/0]_s$; #1 AP-$[\pm 20_4/0]_s$ (no strain data); #1 AP-$[\pm 22.5_3/0_2/\pm 22.5_3]_s$ ($\varepsilon_x = 1.4\%$). All these specimens were tested at 25 s^{-1}. Despite some

slippage occurring, Figure 6 shows that the two specimens behaved similarly to the other specimens tested at that strain rate and so are acceptable representations of the overall behaviour. All specimens were submerged in zinc iodide solution dye penetrant for 24 hours prior to being wiped clean and CT scanned.

All four specimens displayed damage in the form of fragmentations and dispersed delamination, as was observed in [11]. The extent of damage in each one varied but never covered the entire gauge length, indicating that they were not deformed sufficiently to reach fragmentation saturation.

Figures 15 and 16 show the midplane of the AP-$[\pm 26_6/0]_s$ specimens. There are minimal fragmentations and dispersed delaminations in Figure 15, with a single highlighted region extending across the specimen. The predominant damage in this specimen are the free edge delaminations, which cover much of the gauge length. These free edge delaminations have been shown in [11] to occur at the innermost -26/26 interfaces, propagating from the fibre fractures in the 0° plies. Though not visible due to the lack of dispersed delamination, it is understood that fragmentations should be co-located with all the free edge delaminations visualised.
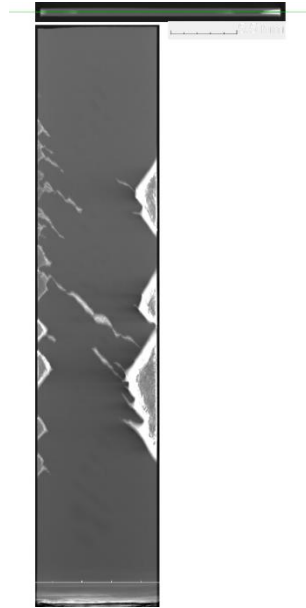
Figure 15: The CT imagery highlights development of fragmentations and dispersed delaminations in the 0° plies of AP-$[\pm26_6/0]_s$ #1 (25 s^{-1}). It also shows the large free edge delaminations that have propagated at the -26/0 interface.

There are considerably more fragmentations and dispersed delaminations in AP-$[\pm26_6/0]_s$ specimen #10 (Figure 16). Data recording issues meant that the strain was not captured, but the specimen certainly reached a higher deformation than #1 (Figure 15). The extent of dispersed delaminations shown in Figure 16 is consistent with the damage accumulation seen in quasi-static specimens that have experienced strains in excess of 2.5% [11]. Similarly to specimen #1, #10 shows multiple free edge delaminations that coincide with fragmentations. The paths of the fragmentations can be identified as thin lines of bright white that are within regions bounded by thicker lines of brightness. In between these areas the 0/- 26 interface has not delaminated.
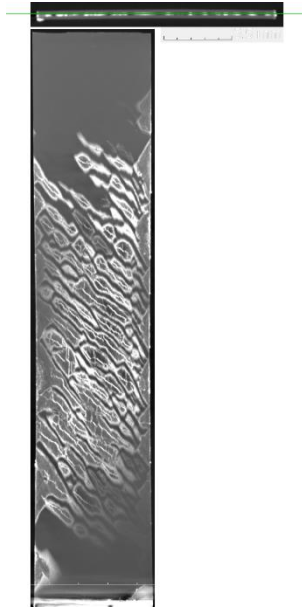
Figure 16: Fragmentations and dispersed delaminations in the 0° plies are much more widespread in this image of AP-$[\pm 26_6/0]_s$ #10. The central area is densely damaged, including the propagation of free edge delaminations.

The appearance of the fragmentations and dispersed delaminations in the AP-$[\pm 20_4/0]_s$ and AP-$[\pm 22.5_3/0_2/\pm 22.5_3]_s$ specimens, as shown in Figures 17 and 18, is different from that discussed for the AP-$[\pm 26_6/0]_s$ specimens. The fragmentations are less inclined to the loading direction and spaced further apart. The majority of the visualised damage does not extend across the entire specimen width. Figure 17 shows that many dispersed delaminations seem to propagate from the edges but do not meet in the middle. This suggests that the fragmentations also do not extend the entire specimen width. It is, however, very likely that the fragmentations do cover the entire width [11]. Without dispersed delaminations to aid the penetration of dye, there is insufficient resolution in the presented scans to confirm this.
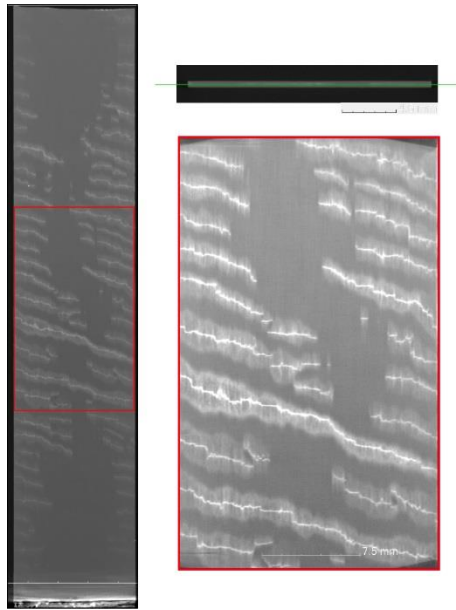
Figure 17: The images show the locations of fragmentations and dispersed delaminations for a AP-[$\pm20_4/0$]$_s$ specimen (#1). The inset image highlights how only two fragmentations are seen to extend the entire width.

Images have been captured of both the 0° ply blocks in the AP-[$\pm22.5_3/0_2/\pm22.5_3$]$_s$ specimens. The thickness location of the scans, indicated by green arrows in Figures 18a and 18b, are at approximately the middle of the 0° two-ply block in the lower and upper halves of the laminate, respectively. The morphology of the damage in this specimen is similar to the last, but there are numerous free-edge delaminations observed, with some large areas in Figure 18b. The extent of the damage in each of the 0° ply blocks is very similar. The spacing of the fractures is consistent, though they cover more of the specimen width in Figure 18b and do not occur in the same location along the gauge length.
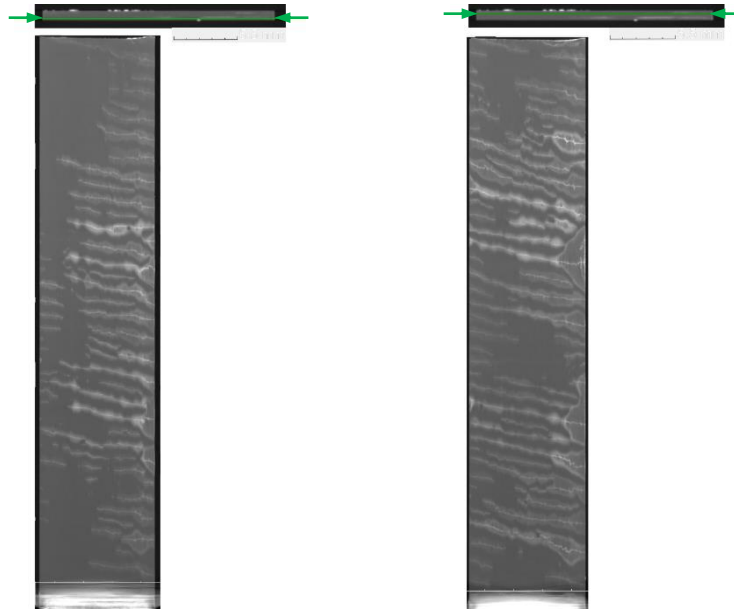
(a) Lower zero position.   *(b) Upper zero position.*

Figure 18: The CT images highlight that fragmentations and delaminations occurred in both zero ply blocks of the AP-$[\pm22.5_3/0_2/\pm22.5_3]_s$ specimen.

4. Conclusions

In this work, the effect of strain rate on the tensile behaviour of pseudo-ductile thin-ply UD, QI and AP composites was studied and the following conclusions are drawn.

- UD and QI hybrid composite laminates have excellent pseudo-ductility responses both in the quasi-static and high strain rates through fragmentation and stable pull-out of the carbon layers, however the angle-plies are strain rate dependent and pseudo-ductility decreases with increasing strain rate.

- For the UD and QI hybrids, all the specimens showed a slight stiffening, in the elastic part of the tests, at high strain rates compared to the quasi-static case. In addition, max-strain and max-stress values were slightly higher for the high strain rates compared to the quasi-static tests.

- Comparing the observed damage mechanisms for the quasi-static and high strain rates, a similar type of damage occurred for the UD and QI specimens, except for the UD-

G/4C/G laminates, where with increasing strain rate, the observed damage mode changes from pure delamination to stable fragmentation/delamination, believed to be due to the increase in mode II interlaminar fracture toughness.

- In the case of the AP configurations, all specimens showed similar initial moduli but then a reduced loss of stiffness compared to the quasi-static case. The rate dependent behaviour was most pronounced for the AP-$[\pm 26_6/0]_s$ specimens with TC35 carbon fibre. The increased off-axis angle leads to higher shear stresses in the AP layers and so more influence from the matrix. The effect of the rate dependence on the stiffness of the AP layers was lessened by the use of high modulus fibres (M55J) in the $0°$ plies, which dominate initial loading. Additionally, a reduced strain in the laminate limited the non-linearity of the AP layers compared to the AP-$[\pm 26_6/0]_s$ case.

- Across all the AP specimens, the strains to failure at high rates were considerably less than recorded for the quasi-static tests. This reduction is thought to be due to the rate dependence of the epoxy matrix that leads to a modification of the shear response of the laminate.

- Microscopy and X-ray CT analysis of the AP specimens that were not loaded to failure, clearly showed evidence of fragmentations and dispersed delaminations. The presence of these mechanisms indicated that damage developed as previously observed in quasi-static testing. Hence, it can be concluded that pseudo-ductility is achievable in thin ply $[\pm \theta_m/0_n]_s$ laminates loaded at high strain rates. Rate effects, however, led to a change in behaviour at the highest rates that affected the development of non-linearity and therefore do need to be taken into account in designing layups.

Acknowledgement

References:

[1] Diao H, Bismarck A, Robinson P, Wisnom MR. Pseudo-ductile behaviour of unidirectional fibre reinforced polyamide-12 composite by intra-tow hybridization. In: Proceedings of ECCM 15 Conference. Venice; June, 2012.

[2] Hayashi T. Development of new material properties by hybrid composition. 1st report. Fukugo Zairyo (Composite Materials) 1972;1:18–20.

[3] Hayashi T, Koyama K, Yamazaki A, Kihira M. Development of new material properties by hybrid composition. 2nd report. Fukugo Zairyo (Composite Materials) 1972;1:21–25.

[4] Bunsell AR, Harris B. Hybrid carbon and glass fibre composites. Composites 1974;5:157–64.

[5] Manders PW, Bader MG. The strength of hybrid glass/carbon fibre composites. J Mater Sci 1981;16:2233–45.

[6] Czél G, Jalalvand M, Wisnom MR. Design and characterisation of advanced pseudo-ductile unidirectional thin-ply carbon/epoxy– glass/epoxy hybrid composites. Compos Struct, V 143:362–370, 2016.

[7] Jalalvand M, Czél G, Wisnom MR. Damage analysis of pseudo-ductile thin-ply UD hybrid composites – A new analytical method. Compos Part A Appl Sci Manuf, 69:83–93, 2015.

[8] Jalalvand M, Czél G, Wisnom MR. Parametric study of failure mechanisms and optimal configurations of pseudo-ductile thin-ply UD hybrid composites. Compos Part A Appl Sci Manuf; 74:123–131, 2015.

[9] Fotouhi M, Jalalvand M, Wisnom MR, High performance quasi-isotropic thin ply carbon/glass hybrid composites with pseudo-ductile behaviour in all fibre orientations, Composites Science and Technology, 152: 101-110, 2017.

[10] Fuller JD, Wisnom MR. Pseudo-ductility and damage suppression in thin ply CFRP angle-ply laminates. Compos Part A Appl Sci Manuf; 69:64–71, 2014.

[11] Fuller JD, Jalalvand M, Wisnom MR, Combining fibre rotation and fragmentation to achieve pseudo-ductile CFRP laminates, Composite Structures; 142: 155-166, 2016.

[12] Sun C, Zhu C, The effect of deformation-induced change of fiber orientation on the non-linear behavior of polymeric composite laminates, Composites science and technology, 60: 2337-2345, 2000.

[13] Weeks C, Sun C, Modeling non-linear rate-dependent behavior in fiber-reinforced composites, Composites Science and Technology, 58(3-4): 603-611, 1998.

[14] Shokrieh MM, Omidi MJ, Tension behavior of unidirectional glass/epoxy composites under different strain rates, Composite Structures, 88(4):595–601, 2009.

[15] Gurusideswar S, Srinivasan N, Velmurugan R, and Guptac NK, Tensile Response of Epoxy and Glass/Epoxy Composites at Low and Medium Strain Rate Regimes, Procedia Engineering, 173, 686-693, 2017.

[16] Elanchezhian C, VijayaRamnath B, Hemalatha J. Mechanical behavior of glass and carbon fibre reinforced composites at varying strain rates and temperatures. Procedia Mater Sci, 6:14, 05-18, 2014.

[17] Harding J, Welsh LM, A tensile testing technique for fibre-reinforced composites at impact rates of strain, Journal of materials science, 18:1810-1826, 1983.

[18] Ochola RO, Marcus K, Nurick GN, Franz T. Mechanical behavior of glass and carbon fibre reinforced composites at varying strain rates. Compos Struct 2004;63:455e67.

[19] Gurusideswar S, Velmurugan R, Gupta NK. High strain rate sensitivity of epoxy/clay nanocomposites using non-contact strain measurement. Polymer 2016; 86:197e207.

[20] Naik NK, Ramasimha R, Arya H, Prabhu SV, ShamaRao N. Impact response and damage tolerance characteristics of glass/carbon hybrid composite plates. Compos Part B Eng 2001;32:565e74.

[21] Naresh K., Shankar K., Rao B.S., Velmurugan R. Effect of high strain rate on glass/carbon/hybrid fiber reinforced epoxy laminated composites, Composites Part B 100 (2016) 125e135.

[22] Daniel IM. High Strain Rate Properties of Angle Ply Composite Laminates. IIT RESEARCH INST CHICAGO IL, 1981.

[23] Cui H, Thomson D, Pellegrino A, Wiegand J, Petrinic N, Effect of strain rate and fibre rotation on the in-plane shear response of ±45° laminates in tension and compression tests, Composites Science and Technology 135 (2016), 106e115.

[24] M. L. Longana, Intermediate strain rate testing methodologies and full-field optical strain measurement techniques for composite materials characterisation. PhD thesis, University of Southampton, 2014.

[25] Wisnom MR, Czél G, Swolfs Y, Jalalvand M, Gorbatikh L, Verpoest I. Hybrid effects in thin ply carbon/glass unidirectional laminates: Accurate experimental determination and prediction. Compos Part A, 88:131-139, 2016.